Investigation of GeV-scale electron acceleration in a gas-filled capillary discharge waveguide

2013 New J. Phys. 15 045024

(http://iopscience.iop.org/1367-2630/15/4/045024)

New Journal of Physics
The open access journal for physics

Investigation of GeV-scale electron acceleration in a gas-filled capillary discharge waveguide

P A Walker[1], N Bourgeois[1], W Rittershofer[1], J Cowley[1], N Kajumba[2], A R Maier[3], J Wenz[2], C M Werle[2], S Karsch[2], F Grüner[3], D R Symes[4], P P Rajeev[4], S J Hawkes[4], O Chekhlov[4], C J Hooker[4], B Parry[4], Y Tang[4] and S M Hooker[1,5]

[1] Department of Physics, University of Oxford, Clarendon Laboratory, Parks Road, Oxford OX1 3PU, UK
[2] Department of Physics, Ludwig-Maximilians-Universität München, D-85748 Garching, Germany
[3] University of Hamburg and Center for Free-Electron Laser Science (CFEL), Luruper Chaussee 149, 22761 Hamburg, Germany
[4] Central Laser Facility, Rutherford Appleton Laboratory, Didcot OX11 0QX, UK
E-mail: simon.hooker@physics.ox.ac.uk

New Journal of Physics **15** (2013) 045024 (17pp)
Received 4 January 2013
Published 26 April 2013
Online at http://www.njp.org/
doi:10.1088/1367-2630/15/4/045024

Abstract. The generation of GeV-scale electron beams in a gas-filled capillary discharge waveguide with good reproducibility is discussed. Beams of electrons with energies above 900 MeV, and with root-mean-square divergences of 3.5 mrad, are observed for a plasma density of 2.2×10^{18} cm^{-3} and a peak input laser power of 55 TW. The variation of the maximum electron energy with the plasma density is measured and found to agree well with simple models. Injection and acceleration of electrons at the to date lowest plasma density of 3.2×10^{17} cm^{-3} are reported. The energy spectra of the generated electron beams exhibit good shot-to-shot reproducibility, with the observed variations attributable to the measured shot-to-shot jitter of the laser parameters. Two methods for correcting the effect of beam pointing variations on the measured energy spectrum are described.

[5] Author to whom any correspondence should be addressed.

Contents

1. Introduction

As first recognized by Tajima and Dawson in 1979 [1], longitudinal plasma waves excited by intense laser pulses contain intense electric fields that are well suited to accelerating charged particles to relativistic energies. This concept was later extended to plasma waves driven by particle beams [2]. For both laser- and beam-driven plasma accelerators, the accelerating electric field is three or four orders of magnitude greater than can be achieved in conventional radio-frequency accelerators, allowing a corresponding reduction in the accelerator length.

Laser-driven plasma accelerators operate in several regimes, depending on the intensity of the driving laser pulse, the density of the plasma and the duration of the laser pulse relative to the plasma period. A comprehensive review of the physics of these regimes has recently been provided by Esarey *et al* [3]. In the experiments reported here, a single laser pulse with a duration less than the plasma period $T_p = 2\pi/\omega_p$ excites a plasma wave via the action of the ponderomotive force; here $\omega_p = (n_e e^2/\gamma m_e \epsilon_0)^{1/2}$ is the angular plasma frequency, n_e is the plasma density and γ is the relativistic factor of the quivering electrons. This force pushes charged particles away from regions of high spatial gradients in the pulse intensity and, as the mass of the plasma ions greatly exceeds that of the plasma electrons, the ions can be considered to remain essentially stationary while the electrons are pushed away from the region of the laser pulse. The resulting charge separation sets up a plasma density wave—known as a plasma wakefield—which trails the laser pulse. The longitudinal electric fields within the plasma wave can reach magnitudes of the order of the cold wave-breaking limit $E_0 = m_e c\omega_p/e$, which for typical plasma densities of order $n_e \approx 10^{18}\,\mathrm{cm}^{-3}$ gives $E_0 \approx 100\,\mathrm{GeV\,m}^{-1}$.

In early work on laser-driven plasma accelerators, the generated electron beams had a very broad energy spectrum, but in 2004 three groups reported the generation of beams with quasi-monoenergetic energy spectra in the 100–200 MeV range. In that work, the target plasma was formed by ionization of a gas jet by the driving laser [4, 5], or a plasma channel formed by additional laser pulses [6]. In 2006 the energy of laser-accelerated electron beams was increased to 1 GeV by channelling the driving laser pulse in the plasma channel formed in a capillary discharge waveguide [7, 8], and subsequently electrons with GeV-scale energies were produced by laser-driven acceleration in the plasma channel [9–12] and in gas jets or gas cells [13–16].

In this paper, we discuss the results of experiments on electron acceleration in plasma channels formed in capillary discharge waveguides. We present the results of a study of the

dependence of the electron energy on the plasma density, and report GeV-scale electron energies produced by laser pulses with a peak power of $P = 55\,\mathrm{TW}$, which is double the laser power employed by Karsch *et al* [9] and Ibbotson *et al* [10, 11] and 40% of the laser power used by Lu *et al* [12]. The shot-to-shot reproducibility of the electron beams is investigated and compared with variations in the parameters of the driving laser pulse. We compare two methods for correcting the electron energy spectra recorded for generated electron beams that propagate at an angle to the spectrometer axis. Finally, we report on injection and acceleration of electrons at the lowest plasma densities reported to date, a result that is promising for future experiments with greater energy gain per stage.

The paper is arranged as follows. In section 2, the benefits of plasma accelerators driven in waveguides are introduced. Section 3 describes in detail the experimental arrangement employed in this work, and the results are presented in section 4.

2. Plasma accelerators driven in waveguides

We first briefly discuss the operation of plasma accelerators driven within a waveguide structure.

In a uniform plasma the phase velocity of a laser-driven plasma wave is close to, but slightly less than, c since the laser pulse propagates with a group velocity $v_g < c$. The small difference in the velocity of the accelerated electrons, which for relativistic energies is very close to c, and the velocity of the plasma wave causes the accelerated electron bunch to outrun the plasma wave. The electron bunch moves from an accelerating phase to a decelerating one after the dephasing length L_d. For nonlinear plasma waves, i.e. wakefields driven by laser pulses with a normalized vector potential $a_0 > 1$, where $a_0 = eA/m_e c$ and A is the vector potential of the laser field, the dephasing length can be written [17] as $L_d = (4/3)(\omega_0^2/\omega_p^3)c\sqrt{a_0}$. Since the peak accelerating field E_0 is proportional to ω_p, the maximum energy gain per stage scales as $W_{max} \propto E_0 L_d \propto 1/\omega_p^2 \propto 1/n_e$. For these reasons there is considerable interest in driving plasma accelerators at lower plasma densities, and over longer distances, thereby yielding higher particle energy gain per accelerator stage.

For low laser intensities, corresponding to $a_0 \ll 1$, a linear wakefield is formed in which the relative amplitude of the plasma wave $\delta n_e/n_e \ll 1$ and the wakefield is sinusoidal [3]. For higher values of a_0, the wake becomes nonlinear and loses its simple sinusoidal form [3]. At still higher values of a_0, the 'blowout' or 'bubble' regime is reached in which the laser pulse expels essentially all the electrons from the axis, leaving an approximately spherical cavity with ideal focusing and accelerating properties [18]. This regime is of particular current interest since electrons from the target plasma can be self-injected at the back of the bubble, and subsequently accelerated to high energy [19]. Reaching the bubble regime requires $a_0 > 2$ and that the laser spot size w_0 is properly matched to the plasma skin depth, i.e. $w_0 = w_{sf} \equiv 2k_p^{-1}\sqrt{a_0}$. Here the spot size is defined for a laser pulse with a Gaussian transverse intensity profile of the form $I(r) = I(0)\exp\left[-2(r/w_0)^2\right]$ in which r is the distance from the axis of propagation.

To reach the high laser intensities needed to drive the bubble regime, it is necessary to focus the laser pulse to a small spot size. However, this also means that the laser pulse will tend to diffract, limiting the distance for which the plasma wave has significant amplitude, and hence the energy gained by particles trapped in the wake. The pulse will diffract significantly over a distance of the order of the Rayleigh range $z_R = \pi w_0^2/\lambda$, where λ is the laser wavelength [20].

Extending the acceleration length beyond the limit set by diffraction requires that the laser pulse be guided by some mechanism. In general, guiding can be achieved if the transverse

refractive index is of the 'step-index' or 'gradient-index' type. Low-loss guiding of high-power laser pulses in step-index waveguides formed by a hollow-core capillary has been demonstrated [21, 22] and the amplitude of plasma waves driven in these structures has been measured [23]. Here we concentrate on gradient-index guiding; this can occur naturally, through variations of the relativistic motion of the plasma electrons, or by providing a plasma channel in which the density of the plasma varies with the transverse coordinate.

The refractive index of a plasma is given by $\eta = \left[1 - (\omega_p^2/\omega_0^2)\right]^{1/2} \approx 1 - n_e e^2/2\gamma m_e \epsilon_0 \omega_0^2$, where the approximation holds if $\omega_0 \gg \omega_p$. Gradient refractive index guiding requires that the transverse refractive index profile is peaked on the propagation axis [24]. A transverse refractive index profile of the correct form develops naturally through the transverse variation of the γ-factor of the plasma electrons oscillating in the driving laser field: since the laser intensity profile is peaked on-axis, γ—and hence η—will also be peaked on-axis. This leads to relativistic self-*focusing* [25] for laser powers $P > P_c \equiv 17.4(\omega_p/\omega_0)^2$ GW. A relativistically self-focused laser pulse will drive a nonlinear plasma wave, and as such will experience longitudinal and transverse variations of the plasma density; at the front of the laser pulse the transverse density profile tends to cancel the effect of relativistic self-focusing, and hence—in the absence of an external waveguide—the front of the pulse diffracts essentially freely [17, 25]. As discussed by Lu *et al* [17], in such cases the laser pulse can still be considered to be effectively self-*guided* if the rate at which the pulse loses energy to driving the plasma wave exceeds the rate at which energy is diffracted away. This leads to a condition for self-guiding of $a_0 > (\omega_0/\omega_p)^{2/5}$; assuming that the pulse is self-focused to the matched self-focused spot size w_{sf}, the condition on the laser power for self-guiding becomes $P \geqslant P_c^{diff} = (1/8)(\omega_0/\omega_p)^{6/5} P_c$. For the parameters of interest in this work, $P_c^{diff} > P_c$ and hence the laser power requirement for self-guiding is significantly greater than that required for self-focusing alone.

For laser powers below P_c^{diff}, the bubble regime can be driven over long distances if the front of the laser pulse is guided by a waveguide. It can be shown [17] that the conditions for reaching the bubble regime—i.e. $a_0 > 2$ and $w_0 \approx w_{sf}$—correspond to $P > P_c$; hence the back of the laser pulse will be focused by relativistic self-focusing and the transverse density profile of the bubble, while the front is guided only by the external waveguide.

In a plasma, a gradient refractive index waveguide is formed if the transverse plasma density profile has a minimum on-axis. Plasma channels of this type have been generated by several methods, including hydrodynamic expansion of a laser-produced spark [26, 27], discharge-ablated capillaries [28], z-pinch capillary discharges [29], open-geometry discharges [30] and gas-filled capillary discharges [31]. In this paper, we will describe experiments on electron acceleration in gas-filled capillary discharge waveguides. Waveguides of this type have been shown [31, 32] to guide laser pulses with peak intensities above $10^{17}\,\mathrm{W\,cm^{-2}}$ over distances up to 50 mm and have been used in several experiments on laser-driven plasma accelerators [7, 9–11, 33], including the generation of GeV electron beams for the first time [7, 8]. The operation of these waveguides has been described in detail previously [34, 35]. Briefly, hydrogen gas flows into a capillary with a diameter of 200–300 μm and tens of millimetres in length. A pulsed discharge, with a peak current of 300–500 A and of approximately 200 ns half-period, flows through the capillary; this ionizes the gas and establishes a plasma channel through thermal conduction of heat to the capillary wall.

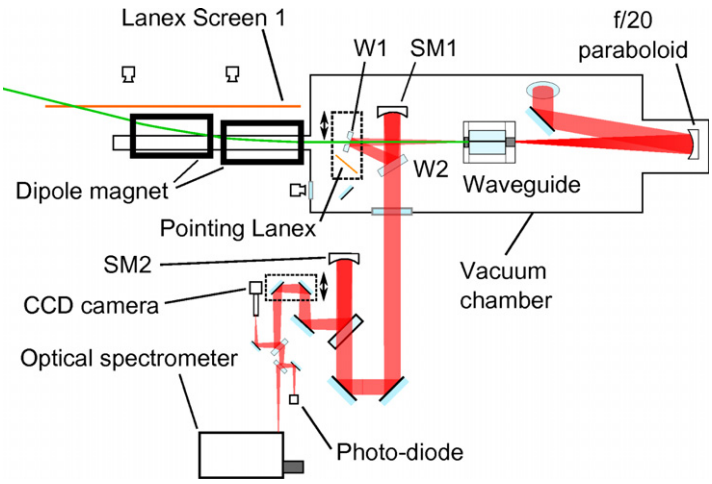

Figure 1. Schematic diagram of the experimental setup employed.

3. Experimental setup

The experiments described here were performed with the North beam of the Astra-Gemini laser using a similar arrangement to earlier work [10], as shown in figure 1.

The Astra-Gemini laser is a dual-beam Ti:sapphire laser system and has been described in detail elsewhere [36]. The two beams, labelled North and South, are compressed in separate compressors; owing to problems with the South compressor, for the experiments described in this paper the amplified South beam was temporally compressed in the North compressor. This required the uncompressed beam to propagate through $\approx$1 m of air which could not be fully shielded against air currents, and this may have increased the shot-to-shot jitter in the on-target beam pointing, which for this experiment was found to be 8 μrad. We note that pointing stabilization systems [37] can reduce this jitter to less than 3 μrad.

Laser pulses were focused on the entrance plane of the capillary waveguide by an off-axis paraboloid of $f = 3$ m focal length used at $f/20$. A soft aperture was placed in the beam, prior to the final laser amplifier, to improve the focal spot quality. As shown in figure 2, this increased the fraction of energy contained within the half-peak-intensity contour of the focal spot from 32 to 38%, which may be compared with a fraction of 50% expected for an ideal Gaussian beam. Apodizing the beam limited the maximum on-target energy to 4.2 J, of which approximately $(0.38/0.5) \times 4.2\,\mathrm{J} = 3.2\,\mathrm{J}$ can be estimated to be contained within the lowest-order Gaussian mode. The soft aperture was used for all measurements reported in this paper; unless stated otherwise, the laser pulse energies and peak powers and intensities given in this paper are the estimated on-target energy contained within the lowest-order Gaussian mode. With the aperture in place the transverse intensity profile of the focal spot was measured to have a full-width at half maximum (FWHM) of 41 μm at the entrance of the capillary. The temporal profile of the incident laser pulse was characterized with a GRENOUILLE [38] from which the FWHM duration of the pulses was determined to be $\tau = 55$ fs. Assuming an effective laser pulse energy of 3.2 J, the maximum incident peak power, focal intensity and normalized vector potential were $P = 55$ TW, $I = 2.9 \times 10^{18}\,\mathrm{W\,cm^{-2}}$ and $a_{0,\mathrm{in}} = 1.1$, respectively.

For these experiments the capillary discharge waveguide employed 33 mm long, 300 μm diameter capillaries laser machined into sapphire blocks [39]. An image of the capillary and

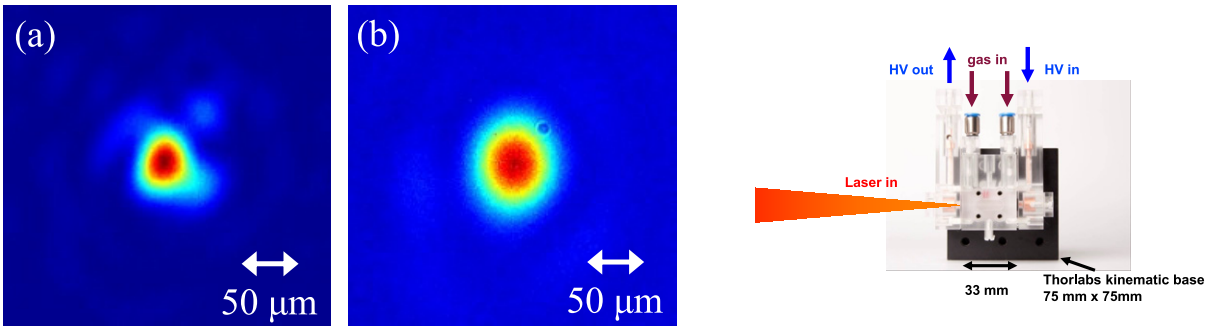

Figure 2. (left) The laser spot recorded at focus without (a) and with (b) a soft aperture placed in the beam prior to the final amplifier. (right) Annotated photograph of the capillary discharge waveguide and its supporting structure.

its support structure is shown in figure 2. The capillary was filled with hydrogen gas via two gas slots of 650 μm diameter located 4 mm from each end of the capillary. The plasma channel was formed by a discharge pulse with a peak current of 500 A and a 200 ns half period. The matched spot size of the channel formed, and the axial plasma density n_e were determined from the initial gas pressure, measured in the gas supply line, and scaling laws deduced from interferometric measurements of square channels [40]. The scaling laws are valid from 0.3×10^{18} to 3.3×10^{18} cm^{-3} for capillaries of diameter 125–465 μm; for a 300 μm diameter capillary and a plasma density of 2.2×10^{18} cm^{-3}, the matched spot size is 46 μm. The estimated error in the axial plasma density from the scaling law is approximately 10% at an axial density of 1×10^{18} cm^{-3}. Note that although the interferometric measurements were performed with square-sided capillaries, numerical simulations show that the cross-sectional shape of the capillary has little effect on the matched spot size and axial electron density of the plasma channel [41].

A 102.6 mm diameter wedge ($W1$), in which a 20 mm diameter hole had been drilled at 45° to the normal, was placed approximately 1.6 m from the exit of the capillary and oriented at 45° to the propagation axis of the laser. Laser light transmitted through the capillary was reflected from the front surface of the wedge onto a second wedge ($W2$) of 254 mm diameter and then to a spherical mirror (SM1) of focal length 2540 mm, arranged so as to retro-reflect and collimate the beam. The collimated beam passed through $W2$ and out of the vacuum chamber, and was refocused using a combination of a wedge and spherical mirror equivalent to that used in the chamber to collimate the beam. Several diagnostics measured the properties of the transmitted laser radiation: (i) a CCD camera to image the transverse intensity profile of the laser in either the entrance or exit plane of the capillary (the object plane being determined by the position of SM1); (ii) a photodiode to measure the transmitted laser energy; (iii) an optical spectrometer; and (iv) a GRENOUILLE to measure the temporal profile of the pulse.

Electrons accelerated within the plasma channel passed through the hole in $W1$ and were dispersed by the magnetic field produced by two permanent dipole magnets. Each dipole magnet produced a field of 0.78 T in a region 0.4 m (parallel to the laser axis) by 0.15 m (horizontal) by 0.04 m (vertical). The dipole magnets were separated by 0.05 m in the direction parallel to the laser axis; the second dipole was offset in the horizontal plane by 0.05 m to increase the path of high-energy electrons in the magnetic field. The deflected electron beams were detected by a 1 m long Lanex screen, the phosphorescence from which was imaged by a pair of CCD

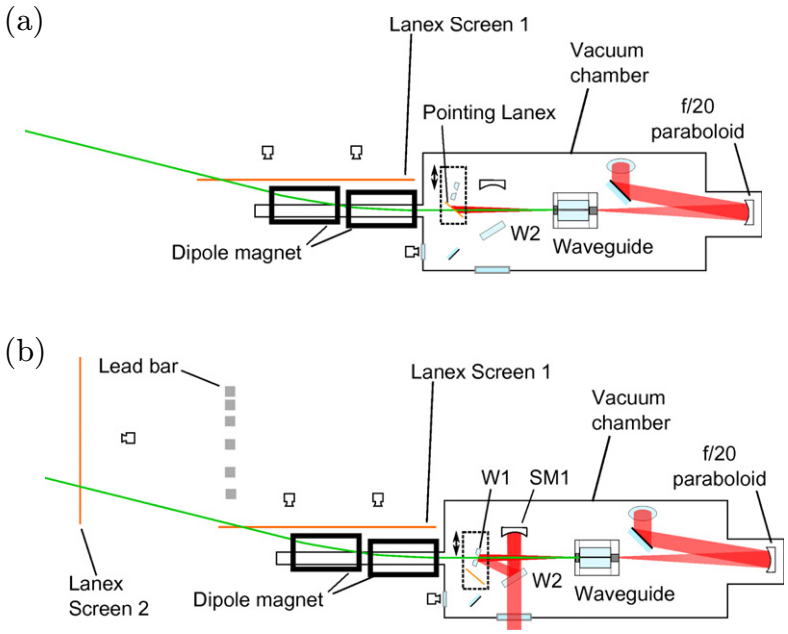

Figure 3. Sketch of the experimental setups of the electron spectrometer to correct for off-axis electron beam propagation using (a) the Pointing Lanex method and (b) the two-screen method.

cameras. Laser light and ambient light from the target area were prevented from entering the cameras objectives by bandpass interference filters with a centre wavelength of 550 nm and a bandwidth of 50 nm.

3.1. Measurement of the electron energy spectrum

As illustrated in figure 3, two dual-screen systems were incorporated to overcome potential errors in the measurement of the electron energy arising from variations in the pointing of the generated electron beams. In the first method, shown in figure 3(a), $W1$ could be replaced by a thin Lanex screen (the 'Pointing Lanex'). The Pointing Lanex comprised a Lanex screen (Kodak, Intensifying Screen Regular) oriented with its back facing the incident electron beam and covered by a 11 μm thick Al foil to block the laser light. Phosphorescence from the front of the Pointing Lanex was imaged by a CCD camera. Since the electron bunch is known to originate within a few μm of the centre of the exit plane of the capillary, measurement of the position of the electron bunch in the plane of the Pointing Lanex yields the position and propagation vector of the beam as it enters the electron spectrometer. From this information, and the known field map of the dipole magnets, the energy calibration of the spectrometer can be calculated for each laser shot.

Figure 3(b) shows an alternative arrangement for beam-pointing correction in which the electron bunch position and propagation vector at the entrance of the spectrometer is deduced from the image of the dispersed electron beam recorded on two screens located *after* the dipole magnets [42, 43]. This method also yields all the information needed to deduce the position and propagation vector of the electron bunch as it enters the magnetic field, although different procedures are required for mono-energetic and broad-band electron spectra. A mono-energetic

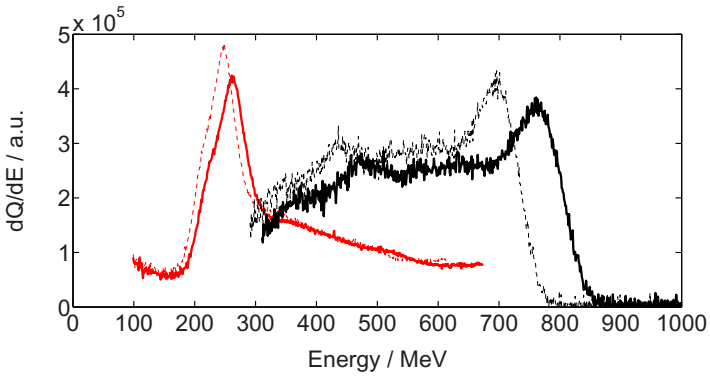

Figure 4. Examples of electron energy spectra recorded before (dashed) and after (solid) correction for off-axis propagation of the electron beam by the Pointing Lanex (black) and two-screen (red) methods on two separate shots.

beam produces a distinct spot on each screen, and since the beam trajectory in this field-free region is a straight line, the position and propagation vector of the beam as it leaves the magnetic field may be deduced. From this information the trajectory through the magnetic field may be calculated for a given electron energy, and hence the apparent position and propagation vector of the electron beam in the exit plane of the capillary can be found. A retrieval algorithm then adjusts the energy of the electron beam until the beam position in the exit plane of the capillary is closest to the centre of the capillary; this yields the energy of the beam and the energy calibration of the spectrometer for that shot.

This approach cannot be used with broad-band electron beams since, in general, the energy spectra have no distinguishing features. To overcome this, lead bars were placed between the two Lanex screens in order to imprint holes in the energy spectrum recorded by the second Lanex screen [44]. The known locations of the lead bars and the measured positions of the spectral holes could then be used to calibrate the spectrometer using the same algorithm used for mono-energetic electron beams. Note that the (corrected) energy spectrum recorded by Lanex Screen 1 is unaffected by the lead bars.

An example of the energy correction determined by the Pointing Lanex method is shown in figure 4. It can be seen that in this case correcting for the off-axis propagation of the electron beam increases the energy of the peak in the electron spectrum from 696 to 765 MeV, an increase of 9.9%. For other shots, correction of the energy spectrum reduced the electron energies: for those shots yielding a positive energy correction, the average increase was 6.4%; for those shots with a negative correction, the average decrease was 2.5%. We note that this method was very easy to implement and, at least for these highly relativistic electron beams, scattering of the electron beam by the Pointing Lanex did not appreciably degrade the recorded energy spectrum on Lanex Screen 1.

Figure 4 shows an example of energy correction using the two-screen method; in this case the correction increases the energy of the peak by 7% to 266 MeV. It is worth noting that for this method it was found that the total beam charge had to be above 20 pC for the spectrum recorded by Lanex Screen 2 to be measurable. Further, if the electron beam propagated at large angles to the system axis it missed the second Lanex screen, preventing correction of the energy spectrum. A further consideration is that the two-screen method requires significant additional

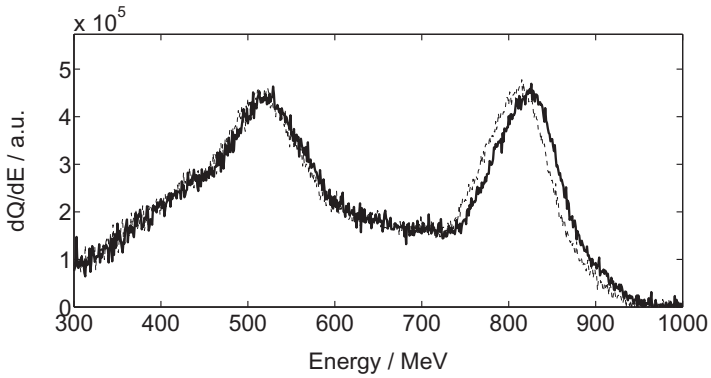

Figure 5. A typical electron spectrum recorded on Lanex Screen 1. The uncorrected spectrum (dashed) is corrected (solid) for off-axis electron beam pointing, but not for variations of the energy or pointing of the incident laser pulse. For this shot the axial plasma density was set to $2.2 \times 10^{18}\,\mathrm{cm}^{-3}$, the laser pulse energy was 3.2 J, the maximum incident peak power and focal intensity were $P = 55\,\mathrm{TW}$ and $I = 2.9 \times 10^{18}\,\mathrm{W\,cm}^{-2}$, respectively, and the laser was timed to arrive within 10.1 ± 2.8 ns of the peak of the discharge current.

space—in our case approximately $1 \times 1\,\mathrm{m}^2$—behind the dipole magnets, and hence overall this method is less convenient.

4. Generated electron beams

Electron energy spectra were recorded for a wide range of axial plasma densities, laser energies, and the delays τ_D between the onset of the discharge and the arrival of the laser. From this initial survey, the optimum conditions for electron beam generation were found to be an axial plasma density of $2.2 \times 10^{18}\,\mathrm{cm}^{-3}$ and the laser pulse timed to arrive at the plasma channel within (10.1 ± 2.8) ns of the peak of the discharge current. The laser pulse energy reaching the capillary, contained within the lowest-order Gaussian beam, was 3.2 J, corresponding to a maximum incident peak power and focal intensity of $P = 55\,\mathrm{TW}$ and $I = 2.9 \times 10^{18}\,\mathrm{W\,cm}^{-2}$, respectively.

Figure 5 presents a typical electron energy spectrum recorded for these conditions, showing two distinct peaks at 512 and 826 MeV. Double-peaked spectra of this type were observed on most shots. The mean peak energies and charges of these were obtained by fitting a double Gaussian distribution to the measured spectra, and were found to be: for the lower-energy peak, (511 ± 77) MeV and (9.2 ± 3.4) pC; for the higher-energy peak, (768 ± 56) MeV and (10.5 ± 3.6) pC.

Dual-peak spectra of this form could arise either by trapping of electrons in two 'buckets' of the plasma wave at different points along the length of the plasma channel, or by hybrid acceleration of the type considered by Hidding *et al* [50] in which the first electron bunch drives its own wakefield which can then accelerate a trailing electron bunch to a higher energy than the first bunch. Particle-in-cell simulations are being undertaken to elucidate the details of the mechanisms responsible for electron trapping and acceleration in our experiments.

For the above-mentioned laser and plasma conditions, the root-mean-square (rms) variation of the beam pointing recorded by the Pointing Lanex was found to be 3.1 mrad. As summarized

Table 1. Summary of measured electron beam divergence and beam pointing fluctuations for selected laser-driven plasma accelerators. The referenced papers are displayed in order of electron energy. For single-shot results and where pointing results were not reported a dash is displayed.

Authors	Method	Energy (MeV)	FWHM divergence (mrad)	rms pointing (mrad)
This paper	◎ S	0991	3.5	3.1
Leemans *et al* [7]	◎ S	1000	1.6[a]	–
Kneip *et al* [13]	⩒ S	0800	3.6[b]	4.0
Ibbotson *et al* [10]	◎ S	540	3.9 (h), 5.4 (v)[b]	4.6 (h), 2.4 (v)
Gonsalves *et al* [45]	◎⩒ D	341	2.5	0.6
Osterhoff *et al* [46]	⊡ S	200	2.1	1.4
Pak *et al* [47]	⩒ S	092	6.0 (h), 12.6 (v)[c]	–
Rechatin *et al* [48]	⩒ C	72	5.0	–
Schmid *et al* [49]	⩒ D	19	7.3	–

Key: ⩒, gas jet; S, self-injection; ⊡, gas cell; C, colliding-pulse injection; ◎, discharge capillary waveguide; D, density-ramp injection.
[a] rms result.
[b] $1/e$ full-width result.
[c] $1/\sqrt{e}$ full-width result.

in table 1, this is similar to previous experiments employing capillary discharge [10], steady-state-flow gas cells [46] and gas jet targets [13], but large compared to the value of 0.57 mrad obtained with an intra-waveguide gas jet to control the electron injection [45].

The divergence of the electron beams could be measured in both the vertical and horizontal directions by the Pointing Lanex, and for the vertical direction by Lanex Screen 1 of the electron spectrometer. For the vertical direction, the two measurements were found to be in agreement. The divergences measured by the Pointing Lanex were $\sigma_{\mathrm{H}} = 3.6$ mrad and $\sigma_{\mathrm{V}} = 3.4$ mrad for the horizontal and vertical planes, respectively, at a plasma density of $n_{\mathrm{e}} = 2.2 \times 10^{18}\,\mathrm{cm}^{-3}$. Note that the laser was polarized in the horizontal direction; previous work has shown [51] that the divergence of the electron beam can be larger in the direction of the electric field of the driving laser as a result of interaction of the accelerating bunch with the tail of the laser pulse. For these conditions the radius of the plasma bubble is $R \approx 2c\sqrt{a_{\mathrm{sf}}}/\omega_{\mathrm{p}} \approx 20\,\mu$m; this is not large compared to the length of the *input* laser pulse, $c\tau = 17\,\mu$m, and hence it might be expected that the electron beams would have a larger divergence in the horizontal plane. That this is not observed to be the case suggests that the laser pulse duration decreases during the long laser–plasma interaction [52]; this conclusion is supported by the fact that for this density the duration of the *transmitted* laser pulse was measured by the GRENOUILLE to be approximately 24 fs.

The reproducibility of the generated electron beams was studied by recording the electron energy spectra for 36 consecutive shots with the same timing and initial gas pressure. Figure 6 shows images of the Lanex Screen 1 for these shots, illustrating that high-energy electron beams were generated on every laser shot with similar electron energy spectra. The spectra have been corrected for variations in the electron beam pointing using the Pointing Lanex

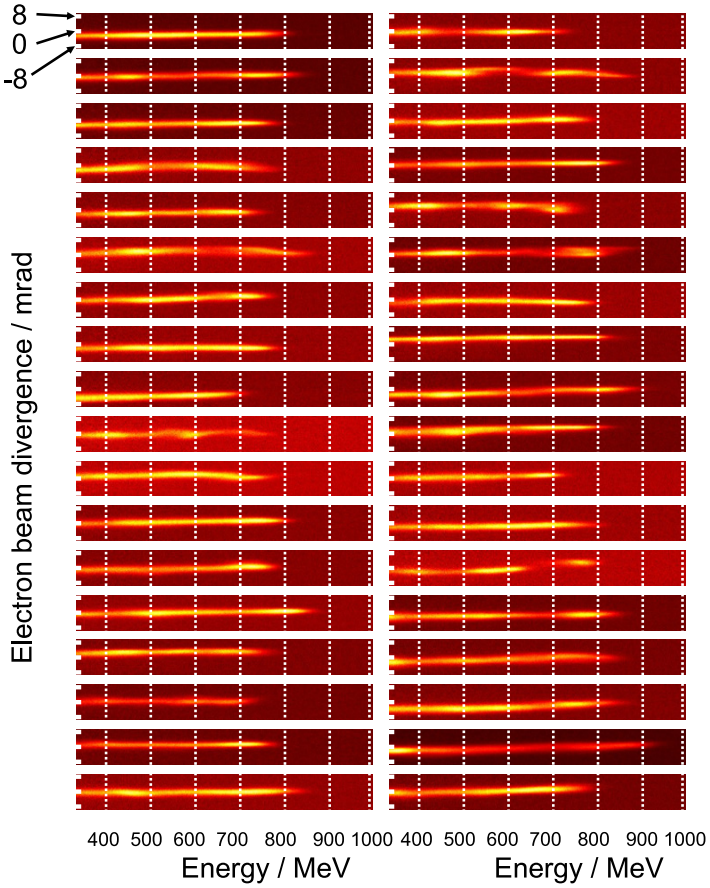

Figure 6. Electron spectra recorded on Lanex Screen 1 for 36 consecutive shots. The vertical axis corresponds to the beam divergence, as illustrated explicitly for the spectrum shown at the top left. These images were corrected for variations of the electron beam pointing but not for variations of the energy or pointing of the incident laser pulse. For these shots the axial plasma density was set to $2.2 \times 10^{18}\,\mathrm{cm}^{-3}$, the laser pulse energy was 3.2 J, the maximum incident peak power and focal intensity were $P = 55\,\mathrm{TW}$ and $I = 2.9 \times 10^{18}\,\mathrm{W\,cm}^{-2}$, respectively, and the laser was timed to arrive within 10.1 ± 2.8 ns of the peak of the discharge current.

method described in section 3.1. However, the spectra have not been corrected for shot-to-shot jitter in the transverse position of the input laser focus, the rms variation of which was measured to be 60% of the laser spot size; or in the laser pulse energy, which had an rms variation of 7.3%. Figure 7 shows the variation of the maximum and peak electron beam energy as a function of laser pulse energy for these 36 shots, showing that, as expected, the electron beam energy increases with the laser pulse energy. A linear fit to the maximum energy data points yields $\mathrm{d}E_{\mathrm{electron}}/\mathrm{d}E_{\mathrm{laser}} = (176 \pm 47)\,\mathrm{MeV\,J}^{-1}$, and hence from the measured standard deviation of the laser pulse energy, $\sigma_{E_{\mathrm{laser}}} = 0.29\,\mathrm{J}$, the variation in the maximum electron energy arising from jitter of the laser energy is expected to be approximately $\sigma_{E_{\mathrm{laser}}}\mathrm{d}E_{\mathrm{electron}}/\mathrm{d}E_{\mathrm{laser}} = (50 \pm 14)\,\mathrm{MeV}$. This is comparable to with the observed standard deviation of the maximum electron energy $\sigma_{E_{\mathrm{electron}}} = 46\,\mathrm{MeV}$. For the data shown in figure 6, the relative rms of the total

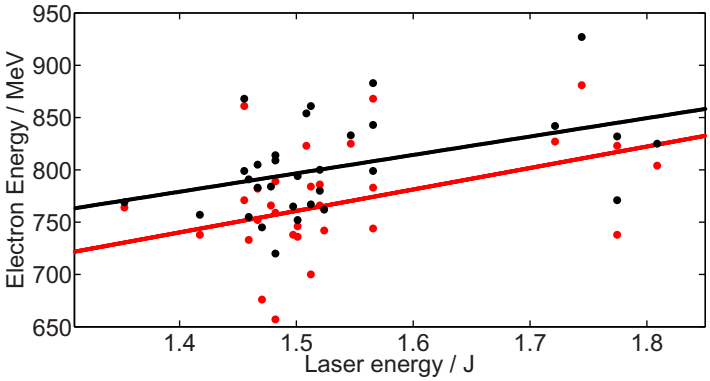

Figure 7. The maximum (black) and peak (red) electron energy as a function of the laser energy within the FWHM of the laser spot. The solid lines are linear fits to the data points. For 5 of the 36 laser shots, the laser control software reported an incorrect laser energy of 0 J; these data were excluded from the above figure.

measured electron charge was $\sigma_Q/\langle Q\rangle = 35\%$. Variations in the pointing of the laser pulse will have caused additional variations in the energy spectra and charge of the accelerated bunches, and it therefore seems likely that the observed shot-to-shot variation of the properties of the electron bunches largely arises from shot-to-shot jitter in the laser parameters.

4.1. Electron energy scaling

The maximum recorded electron energy as a function of the axial plasma density n_e is shown in figure 8. For these shots the laser pulse energy within the lowest-order mode was 3.6 J, the maximum incident peak power and focal intensity were $P = 62$ TW and $I = 3.2 \times 10^{18}$ W cm^{-2}, respectively, and the laser was timed to arrive within 10.1 ± 2.8 ns of the peak of the discharge current. Acceleration is observed in three regimes [10, 17]: (i) at high plasma densities $P > P_c^{\rm diff}$, and hence the plasma channel plays little role in guiding the laser pulses; (ii) a hybrid regime for which $P_c < P < P_c^{\rm diff}$; and (iii) a low-density regime in which $P < P_c$ and hence only the plasma channel can guide the laser pulse.

The expected [17] electron energy after acceleration over one dephasing length, $W_{\rm max} = 2/3\ (m_e c^2/e) a_0\ (\omega_0/\omega_p)^2$, is shown in figure 8 assuming a value of a_0 corresponding to (i) the input laser pulse and (ii) self-consistent relativistic focusing to the matched spot size $w_{\rm sf} = 2k_p^{-1}\sqrt{a_0}$, corresponding [10] to $a_0 = a_{\rm sf} = 2(P/P_c)^{1/3}$. It can be seen that for $n_e \gtrsim 7 \times 10^{17}$ cm^{-3} the measured maximum electron energy lies between these two curves. The fact that the measured energies lie above those predicted for the input a_0 demonstrates that in this regime self-focusing and pulse compression increase the peak vector potential above the input value. That they lie below the energies expected for $a_0 = a_{\rm sf}$ is consistent with coupling losses into the plasma channel, and loss of laser energy to the plasma wave. Also shown in figure 8 is the variation of $W_{\rm max}$ after the laser pulse energy is reduced by the measured energy transmission and allowing for relativistic self-focusing; it can be seen that this simple correction to the expected maximum electron energy significantly improves the agreement with the measured data.

The variation of maximum electron energy shown in figure 8 exhibits a clear optimum plasma density, $n_e^{\rm opt} \approx 0.8 \times 10^{18}$ cm^{-3}, at which electrons with energies up to 991 MeV are

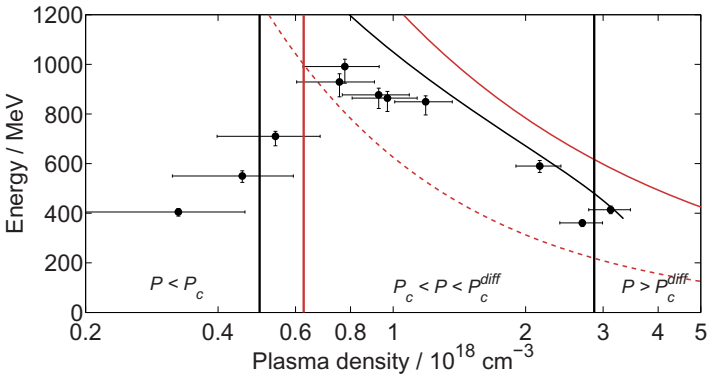

Figure 8. The maximum recorded electron energy as a function of the axial plasma density. The density for which the dephasing length equals the capillary length is shown by the vertical red line. The three different regimes ($P > P_c^{\mathrm{diff}}$, $P_c < P < P_c^{\mathrm{diff}}$ and $P < P_c$) are separated by vertical solid black lines. The dashed red line shows the expected electron energy after acceleration over one dephasing length, assuming a laser pulse with an energy of 3.6 J within the lowest-order mode; the solid red line is the energy gain assuming the laser self-focuses to the matched spot size in the bubble regime [10, 17]. The solid black line represents the energy gain when the transmission of laser energy through the capillary is accounted for as well as self-focusing of the laser pulse. For these data the laser pulse energy within the lowest-order mode was 3.6 J, the maximum incident peak power and focal intensity were $P = 62$ TW and $I = 3.2 \times 10^{18}$ W cm^{-2}, respectively, and the laser was timed to arrive within 10.1 ± 2.8 ns of the peak of the discharge current. The energy error bars result from the unknown pointing of the electron beam (the pointing-correction systems were not in place when these data were taken), which was assumed to be ± 3.1 mrad, i.e. equal to that measured earlier with the Pointing Lanex. The pressure error bars result from the measurement error of the pressure.

observed. This optimum plasma density may be understood as follows. For high plasma densities, the length of the plasma channel L_c is longer than the dephasing length, and in this regime the maximum electron energy will be attained by those electrons trapped in the plasma wave approximately one dephasing length from the capillary exit. Decreasing the plasma density from high values will increase the output electron energy, as observed, until the plasma density corresponds to $L_c \approx L_d$. As shown in figure 8, this condition occurs for plasma densities close to n_e^{opt}; the highest electron energies are obtained for slightly higher plasma densities, which makes sense if at these densities electron injection occurs a short distance after the start of the plasma channel. As the plasma density decreases below the optimum value, both the accelerating electric field and the ratio of the capillary length to L_d will decrease, and hence the electron energy will decrease from that obtained when $L_c \approx L_d$.

It is noteworthy that electron beams were generated for plasma densities as low as 3.25×10^{17} cm^{-3}, as can be seen in figure 8; the bunch charge measured at this plasma density was 5.1 pC. To our knowledge, this is the lowest density at which electron injection and acceleration have been observed. Analysis of experimental results by Mangles and co-workers

[53, 54] and theoretical calculations by Tsung *et al* [55] and Lu *et al* [17, 56] predict that the threshold for self-injection is $a_0 \geqslant 3$. Given the relatively low value of the normalized vector potential of the input pulse ($a_{0,\mathrm{in}} = 1.1$), it is apparent that self-injection could only occur in our experiment if the laser pulse experiences substantial self-focusing and pulse compression. However, at this low density self-focusing only increases the normalized vector potential to $a_0 \approx 1.7$ and laser pulse compression was measured to be of the order of 10%. An alternative analysis [57] of the threshold condition predicts that for our conditions the input laser pulse energy would have to exceed 190 J for self-injection to occur. Hence it is clear that self-injection could not occur in our experiment at the lowest plasma densities for which electron beams were observed, and instead another mechanism, such as ionization injection [33, 47, 58], must play a role. Numerical simulations are in progress to seek insight into the mechanisms responsible for electron injection and the dynamics of acceleration over the long laser–plasma interaction lengths achieved in these experiments. Finally, we note that if for this lowest density the length of the plasma channel were properly matched to the dephasing length of 80 mm, electrons would be accelerated to energies significantly above 1 GeV.

5. Conclusions

In conclusion, the Astra-Gemini laser was used to study electron acceleration in plasma channels formed in a capillary discharge waveguide. Electron beams were generated under conditions corresponding to self-guiding, hybrid guiding and pure plasma channel guiding. At optimal conditions the average electron beam energy was above 900 MeV. The variation of the maximum electron beam energy with the plasma density was found to be in reasonable agreement with simple estimates of acceleration and deceleration in a plasma channel. Details of the mechanisms responsible for electron injection and acceleration over the long lengths of laser–plasma possible in this experiment will be investigated in future work through particle-in-cell simulations.

The energy spectra of the generated electron beams were found to be reasonably reproducible, with the observed shot-to-shot variations being attributable in large part to fluctuations in the properties of the driving laser pulses.

Two methods for correcting the effects on the measured energy spectrum of off-axis electron beam propagation were demonstrated successfully, and for the conditions of this experiment yielded energy corrections of about 10%. Of the two methods, the use of a Pointing Lanex was found to be particularly convenient, and was found not to degrade the recorded energy spectrum.

Acknowledgments

The authors thank M S Bloom, M J V Streeter, S Kneip, Z Najmudin and S P D Mangles from Imperial College, London for their assistance in setting up and calibrating shared diagnostics; and P Brummit, A Zayyani, D Rathbone, D Neville and D Rose from the Rutherford Appleton Laboratory for preparing the target chamber, and drive and gas systems. This work was made possible by financial support from the UK Engineering and Physical Sciences Research Council (grant numbers EP/H011145/1, EP/G067791/1 and EP/F020120/1), the Leverhulme Trust and the Munich-Centre for Advanced Photonics (MAP).

References

[1] Tajima T and Dawson J M 1979 Laser electron-accelerator *Phys. Rev. Lett.* **43** 267–70

[2] Katsouleas T 1986 Physical mechanisms in the plasma wake-field accelerator *Phys. Rev.* A **33** 2056–64

[3] Esarey E, Schroeder C B and Leemans W P 2009 Physics of laser-driven plasma-based electron accelerators *Rev. Mod. Phys.* **81** 1229–85

[4] Mangles S P D *et al* 2004 Monoenergetic beams of relativistic electrons from intense laser–plasma interactions *Nature* **431** 535–8

[5] Faure J, Glinec Y, Pukhov A, Kiselev S, Gordienko S, Lefebvre E, Rousseau J P, Burgy F and Malka V 2004 A laser–plasma accelerator producing monoenergetic electron beams *Nature* **431** 541–4

[6] Geddes C G R, Tóth C, van Tilborg J, Esarey E, Schroeder C B, Bruhwiler D, Nieter C, Cary J and Leemans W P 2004 High-quality electron beams from a laser wakefield accelerator using plasma-channel guiding *Nature* **431** 538–41

[7] Leemans W P, Nagler B, Gonsalves A J, Tóth C S, Nakamura K, Geddes C G R, Esarey E, Schroeder C B and Hooker S M 2006 GeV electron beams from a centimetre-scale accelerator *Nature Phys.* **2** 696–9

[8] Nakamura K, Nagler B, Toth Cs, Geddes C G R, Schroeder C B, Esarey E, Leemans W P, Gonsalves A J and Hooker S M 2007 GeV electron beams from a centimeter-scale channel guided laser wakefield accelerator *Phys. Plasmas* **14** 056708

[9] Karsch S *et al* 2007 GeV-scale electron acceleration in a gas-filled capillary discharge waveguide *New J. Phys.* **9** 415

[10] Ibbotson T P A *et al* 2010 Laser-wakefield acceleration of electron beams in a low density plasma channel *Phys. Rev. Spec. Top. Accel. Beams* **13** 031301

[11] Ibbotson T P A *et al* 2010 Investigation of the role of plasma channels as waveguides for laser-wakefield accelerators *New J. Phys.* **12** 045008

[12] Lu H *et al* 2011 Laser wakefield acceleration of electron beams beyond 1 GeV from an ablative capillary discharge waveguide *Appl. Phys. Lett.* **99** 091502

[13] Kneip S *et al* 2009 Near-GeV acceleration of electrons by a nonlinear plasma wave driven by a self-guided laser pulse *Phys. Rev. Lett.* **103** 035002

[14] Mo M Z, Ali A, Fourmaux S, Lassonde P, Kieffer J C and Fedosejevs R 2012 Quasimonoenergetic electron beams from laser wakefield acceleration in pure nitrogen *Appl. Phys. Lett.* **100** 074101

[15] Liu J S *et al* 2011 All-optical cascaded laser wakefield accelerator using ionization-induced injection *Phys. Rev. Lett.* **107** 035001

[16] Pollock B *et al* 2011 Demonstration of a narrow energy spread, ≈0.5 GeV electron beam from a two-stage laser wakefield accelerator *Phys. Rev. Lett.* **107** 045001

[17] Lu W, Tzoufras M, Joshi C, Tsung F S, Mori W B, Vieira J, Fonseca R A and Silva L O 2007 Generating multi-GeV electron bunches using single stage laser wakefield acceleration in a 3D nonlinear regime *Phys. Rev. Spec. Top. Accel. Beams* **10** 061301

[18] Mori W B 1997 The physics of the nonlinear optics of plasmas at relativistic intensities for short-pulse lasers *IEEE J. Quantum Electron.* **33** 1942–53

[19] Pukhov A and Meyer-ter-Vehn J 2002 Laser wake field acceleration: the highly nonlinear broken-wave regime *Appl. Phys.* B **74** 355–61

[20] Hooker S M and Webb C E 2010 *Laser Physics* (Oxford: Oxford University Press)

[21] Dorchies F *et al* 1999 Monomode guiding of 10^{16} W cm^{-2} laser pulses over 100 Rayleigh lengths in hollow capillary dielectric tubes *Phys. Rev. Lett.* **82** 4655–8

[22] Cros B, Courtois C, Matthieussent G, Di Bernardo A, Batani D, Andreev N and Kuznetsov S 2002 Eigenmodes for capillary tubes with dielectric walls and ultraintense laser pulse guiding *Phys. Rev.* E **65** 026405

[23] Wojda F *et al* 2009 Laser-driven plasma waves in capillary tubes *Phys. Rev.* E **80** 066403

[24] Sprangle P and Esarey E 1992 Interaction of ultrahigh laser fields with beams and plasmas *Phys. Fluids* B **4** 2241–8

[25] Esarey E, Sprangle P, Krall J and Ting A 1997 Self-focusing and guiding of short laser pulses in ionizing gases and plasmas *IEEE J. Quantum Electron.* **33** 1879–914
[26] Durfee C G, Lynch J and Milchberg H M 1995 Development of a plasma waveguide for high-intensity laser pulses *Phys. Rev.* E **51** 2368–89
[27] Volfbeyn P, Esarey E and Leemans W P 1999 Guiding of laser pulses in plasma channels created by the ignitor-heater technique *Phys. Plasmas* **6** 2269–77
[28] Zigler A, Greenberg B, Palhan T, Kaganovich D, Hubbard R F, Ting A, Jones T G and Sprangle P 2002 Ablative and discharge capillaries for optical guiding and velocity control *AIP Conf. Proc.* **647** 47–53
[29] Hosokai T *et al* 2006 Observation of strong correlation between quasimonoenergetic electron beam generation by laser wakefield and laser guiding inside a preplasma cavity *Phys. Rev.* E **73** 036407
[30] Bendoyro R A, Onofrei R I, Sampaio J, Macedo R, Figueira G and Lopes N C 2008 Plasma channels for electron accelerators using discharges in structured gas cells *IEEE Trans. Plasma Sci.* **36** 1728–33
[31] Spence D J and Hooker S M 2001 Investigation of a hydrogen plasma waveguide *Phys. Rev.* E **63** 015401
[32] Butler A, Spence D J and Hooker S M 2002 Guiding of high-intensity laser pulses with a hydrogen-filled capillary discharge waveguide *Phys. Rev. Lett.* **89** 185003
[33] Rowlands-Rees T P *et al* 2008 Laser-driven acceleration of electrons in a partially ionized plasma channel *Phys. Rev. Lett.* **100** 105005
[34] Bobrova N A, Esaulov A A, Sakai J-I, Sasorov P V, Spence D J, Butler A, Hooker S M and Bulanov S V 2001 Simulations of a hydrogen-filled capillary discharge waveguide *Phys. Rev.* E **65** 016407
[35] Broks B H P, Garloff K and van der Mullen J J A M 2005 Nonlocal-thermal-equilibrium model of a pulsed capillary discharge waveguide *Phys. Rev.* E **71** 016401
[36] Hooker C J *et al* 2006 The Astra Gemini project—a dual-beam petawatt Ti:sapphire laser system *J. Physique* IV **133** 673–7
[37] Genoud G, Wojda F, Burza M, Persson A and Wahlstrom C-G 2011 Active control of the pointing of a multi-terawatt laser *Rev. Sci. Instrum.* **82** 033102
[38] O'Shea P, Kimmel M, Gu X and Trebino R 2001 Highly simplified device for ultrashort-pulse measurement *Opt. Lett.* **26** 932–4
[39] Jaroszynski D A *et al* 2006 Radiation sources based on laser-plasma interactions *Phil. Trans. R. Soc.* A **364** 689–710
[40] Gonsalves A J, Rowlands-Rees T P, Broks B H P, van der Mullen J J A M and Hooker S M 2007 Transverse interferometry of a hydrogen-filled capillary discharge waveguide *Phys. Rev. Lett.* **98** 025002
[41] Broks B H P, Van Dijk W, van der Mullen J J A W, Gonsalves A J, Rowlands-Rees T P and Hooker S M 2007 Modeling of a square pulsed capillary discharge waveguide for interferometry measurements *Phys. Plasmas* **14** 023501
[42] Blumenfeld I *et al* 2007 Energy doubling of 42 GeV electrons in a metre-scale plasma wakefield accelerator *Nature* **445** 741–4
[43] Pollock B B *et al* 2009 Two-screen method for determining electron beam energy and deflection from laser wakefield acceleration. *Proc. Particle Accelerator Conf.* (*Vancouver, Canada*) pp 3035–7
[44] Clayton C E *et al* 2010 Self-guided laser wakefield acceleration beyond 1 GeV using ionization-induced injection *Phys. Rev. Lett.* **105** 105003
[45] Gonsalves A J *et al* 2011 Tunable laser plasma accelerator based on longitudinal density tailoring *Nature Phys.* **7** 862–6
[46] Osterhoff J *et al* 2008 Generation of stable, low-divergence electron beams by laser-wakefield acceleration in a steady-state-flow gas cell *Phys. Rev. Lett.* **101** 085002
[47] Pak A, Marsh K A, Martins S F, Lu W, Mori W B and Joshi C 2010 Injection and trapping of tunnel-ionized electrons into laser-produced wakes *Phys. Rev. Lett.* **104** 025003
[48] Rechatin C, Faure J, Lifschitz A, Davoine X, Lefebvre E and Malka V 2009 Quasi-monoenergetic electron beams produced by colliding cross-polarized laser pulses in underdense plasmas *New J. Phys.* **11** 013011

[49] Schmid K, Buck A, Sears C M S, Mikhailova J M, Tautz R, Herrmann D, Geissler M, Krausz F and Veisz L 2010 Density-transition based electron injector for laser driven wakefield accelerators *Phys. Rev. Spec. Top. Accel. Beams* **13** 091301

[50] Hidding B, Königstein T, Osterholz J, Karsch S, Willi O and Pretzler G 2010 Monoenergetic energy doubling in a hybrid laser–plasma wakefield accelerator *Phys. Rev. Lett.* **104** 195002

[51] Mangles S P D *et al* 2006 Laser-wakefield acceleration of monoenergetic electron beams in the first plasma-wave period *Phys. Rev. Lett.* **96** 215001

[52] Schreiber J, Bellei C, Mangles S P D, Kamperidis C, Kneip S, Nagel S R, Palmer C A J, Rajeev P P, Streeter M J V and Najmudin Z 2010 Complete temporal characterization of asymmetric pulse compression in a laser wakefield *Phys. Rev. Lett.* **105** 235003

[53] Mangles S P D, Thomas A G R, Lundh O, Lindau F, Kaluza M C, Persson A, Wahlstrom C G, Krushelnick K and Najmudin Z 2007 On the stability of laser wakefield electron accelerators in the monoenergetic regime *Phys. Plasmas* **14** 056702

[54] Mangles S P D, Thomas A G R, Bellei C, Dangor A E, Kamperidis C, Kneip S, Nagel S R, Willingale L and Najmudin Z 2008 Self-guided wakefield experiments driven by petawatt-class ultrashort laser pulses *IEEE Trans. Plasma Sci.* **36** 1715–21

[55] Tsung F S, Ritesh Narang, Mori W B, Joshi C, Fonseca R A and Silva L O 2004 Near-GeV-energy laser-wakefield acceleration of self-injected electrons in a centimeter-scale plasma channel *Phys. Rev. Lett.* **93** 185002

[56] Lu W, Huang C, Zhou M, Tzoufras M, Tsung F S, Mori W B and Katsouleas T 2006 A nonlinear theory for multidimensional relativistic plasma wave wakefields *Phys. Plasmas* **13** 056709

[57] Mangles S P D, Genoud G, Bloom M S, Burza M, Najmudin Z, Persson A, Svensson K, Thomas A G R and Wahlström C-G 2012 Self-injection threshold in self-guided laser wakefield accelerators *Phys. Rev. Spec. Top. Accel. Beams* **15** 011302

[58] McGuffey C *et al* 2010 Ionization induced trapping in a laser wakefield accelerator *Phys. Rev. Lett.* **104** 025004